IEEE Photonics Journal
An IEEE Photonics Society Publication

Open Access

Active Photonic Band-Gap Switch Based on GaInNAs Multiquantum Well

Volume 4, Number 5, October 2012

Giovanna Calò
Dimitris Alexandropoulos
Vincenzo Petruzzelli

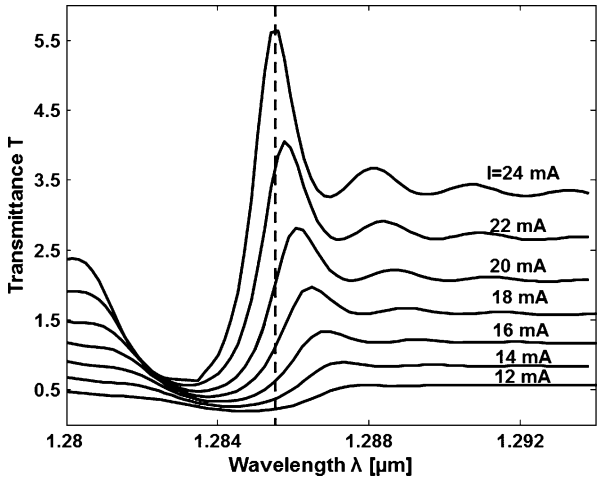

DOI: 10.1109/JPHOT.2012.2220128
1943-0655/$31.00 ©2012 IEEE

Active Photonic Band-Gap Switch Based on GaInNAs Multiquantum Well

Giovanna Calò,[1] Dimitris Alexandropoulos,[2] and Vincenzo Petruzzelli[1]

[1]Dipartimento di Elettrotecnica ed Elettronica, Politecnico di Bari, 70125 Bari, Italy
[2]Department of Materials Science, University of Patras, Patras 26504, Greece

DOI: 10.1109/JPHOT.2012.2220128
1943-0655/$31.00 ©2012 IEEE

Manuscript received July 23, 2012; revised September 15, 2012; accepted September 18, 2012. Date of current version October 4, 2012. This work was supported in part by the Photonic Interconnect Technology for Chip Multiprocessing Architectures ("PHOTONICA") project under the Fondo per gli Investimenti della Ricerca di Base 2008 ("FIRB") program funded by the Italian government and in part by the project "Regional laboratory for synthesis and characterization of new organic and nanostructured materials for electronics, photonics, and advanced technologies" funded by the Apulia Region. Corresponding author: V. Petruzzelli (e-mail: petruzzelli@poliba.it).

Abstract: GaInNAs has been introduced to design an active switch operating at wavelength $\lambda = 1.2855$ μm having high selectivity. The device is made of a mono-dimensional periodic photonic band-gap structure constituted by alternating ridge waveguide layers with different ridge heights. The periodic waveguiding structure has been designed to show the band gap in correspondence of the wavelength range where the dilute nitride active material experiences maximum gain. As an example, the performances of the switch under electrical control are crosstalk CT $= -14.1$ dB, gain in the ON-state G $= 7.6$ dB, and bandwidth $\Delta\lambda_{-10\,\mathrm{dB}} = 1.5$ nm. By increasing the input power above the optical threshold value of the gain saturation, the switching performance worsens in terms of crosstalk and gain, but the wavelength selectivity improves, since the bandwidth decreases down to $\Delta\lambda_{-10\,\mathrm{dB}} = 0.8$ nm for the input optical power $P_i = 20$ mW.

Index Terms: Photonic crystals, quantum well devices, semiconductor materials, optical switches.

1. Introduction

Optical switching functionalities are indispensable for the evolution of optical wavelength division multiplexing systems toward optical terabit networks [1]. This is reflected in the plurality of proposed switching technologies reported in literature in both active and passive configurations that include III–V's, polymers, and silicon substrates. The same applies for the underlying phenomena responsible for the switching mechanism. Optical switches, which take advantage of thermooptic effects [2], electrooptic effects [3], free-carrier dispersion [4], [5], and semiconductor nonlinearities [6], have been demonstrated. Irrespective of the physical mechanism or photonic structure used for the realization of switching, the ideal optical switch should perform fast switching with high ON–OFF ratio, with low-power requirements, and also, it should be integrable. It has been demonstrated recently that photonic band-gap devices (PBG) based on periodic structures such as photonic crystals (PhC) can accommodate these requirements and are therefore a realistic technological solution for optical switching [7]–[9].

PBG devices are an efficient tool of light manipulation at spatial scales that favor miniaturization. PBG structures are characterized by the periodic modulation of the refractive indices, which is able to inhibit the propagation of light at given wavelengths. With the appropriate perturbation of the PBG, it is possible to localize the mode. This PBG attribute has been exploited for the realization of

optical devices such as waveguides, cavities, and filters [10]–[12] even by using nonconventional microstruttured optic fibers [13], [14]. Exploiting the different material properties, the PBG structures can lead to interesting devices such as efficient tunable filters and frequency converters, e.g., in the case of liquid crystal infiltration or nonlinear materials [15]–[17]. Due to their capability of reducing the group velocity at certain wavelengths, PBGs also exhibit a more efficient interaction between the light and the active materials [18], [19].

In this paper, we differentiate from previous approaches to demonstrate the potential of new class of III–V materials, namely, dilute nitrides, in connection with periodic waveguiding structures for switching applications in the second window of the fiber optics telecommunications.

Dilute nitrides or III–V–N compounds offer versatility in band structure engineering. The insertion of nitrogen into III–V semiconductors allows contemporarily reducing the electronic band gap and the lattice constant. This peculiar behavior, specific to III–V–N compounds, leads to the possibility of tailoring both the electronic band gap and the band alignments [20], whereas in conventional III–V compounds, the reduction of the band-gap energy is generally obtained by inserting an element that causes an increase in the lattice constant. By virtue of the design flexibility offered by dilute nitrides, several applications have been demonstrated, such as solar cells [21], semiconductor optical amplifiers (SOA) [22], and light sources, e.g., vertical-cavity surface-emitting lasers (VCSELs) [23], ridge lasers [24], and disk lasers [25], [26].

In particular, GaInNAs compounds have received growing interest in the last decade due to their potentiality for active device applications at the operating wavelength $\lambda = 1.3\ \mu$m. The large conduction band offset induced by the introduction of only a small fraction of nitrogen in the InGaAs matrix leads to an efficient electron confinement in the quantum well (QW). The massive reduction in band gap, achieved due to nitrogen incorporation, enables the growth of very deep GaInNAs–GaAs wells, which trap the carriers at elevated temperatures more efficiently than InP-based materials, and hence, temperature-insensitive operation is feasible [27], [28]. In particular, as [28] reports, both the ASE intensity and the gain coefficient of GaInNAs optical amplifiers showed much less dependence on temperature than those measured for the conventional InP-based corresponding devices. Moreover, for GaInNAs lasers [29], large band-gap materials such as GaInP and AlGaAs can be used for the cladding layer, thus allowing the effective reduction of the carrier overflow at high temperature, leading to better temperature characteristics. These results demonstrate the superior temperature characteristics of the GaInNAs SOA compared with conventional InP-based SOAs.

The temperature independence of the GaInNAs multi-QWs (MQWs) make these compounds particularly interesting for integrated optics compared with conventional optoelectonic devices based on InP technology [30]. In fact, the use of GaInNAs addresses the heating effects that can potentially hinder performance of photonic integrated circuits that are otherwise tackled with bulky solutions such as peltier coolers.

A further interesting feature of GaInNAs-based MQWs is the possibility to achieve polarization insensitivity, thus assuring equal gain for both TE and TM modes, as demonstrated in [22] for GaInNAs–GaInAs MQWs. This polarization insensitivity is important, particularly in telecommunication application in which the active device is used to amplify or switch optical signals whose polarization is randomized due to propagation in conventional optical fibers.

By combining the advantages of the electronic band-gap engineering of dilute nitrides with the capability of tailoring the light propagation by the PBG occurrence, we can tune the optical device characteristics to the applications' requirements, such as wavelength selectivity in WDM optical communication systems.

In this paper, we analyze the gain behavior of active ridge waveguides, based on GaInNAs–GaInAs MQW, patterned with a periodic 1-D grating. The presence of the periodic variation of the waveguide geometry and the consequent occurrence of the PBG can strongly influence the gain behavior [19]. In previous works, we analyzed the switching mechanism that occurs in active defective structures, exploiting conventional III–V compounds, i.e., InGaAsP/InP [31], and novel III–V–N ones, i.e., GaInNAs–GaInAs MQW [32]. In the previously proposed devices, only the defective region was considered active, and their behavior was analyzed under electrical control

and below the optical threshold value of the gain saturation. Here, we investigate both the gain behavior and the wavelength selective switching capability of a completely periodic structure, which is made wholly active by current injection in a GaInNAs–GaInAs MQW. In particular, we focus on the effect of the current variation on the spectral behavior of the periodic structure, which leads to the switching functionality, and on the effect of the optical gain saturation.

2. Brief Theory

The design of the active switch has been carried out by analyzing the electromagnetic (EM) propagation by means of the Bidirectional Beam Propagation Method based on Method of Lines (MoL-BBPM), a robust technique for the EM propagation modeling able to analyze the propagation step by step along the structure [33]–[35]. In this way, some effects such as the injection of current in the active layers can be easily accounted for. In particular, the PBG waveguide was analyzed by a proprietary code based on the MoL-BBPM. This algorithm calculates both the forward $(+z)$ and backward $(-z)$ propagations along the longitudinal z-direction of the waveguide structure. Moreover, at the discontinuities between two alternating layers along the grating structures, from the knowledge of the incident wave, it is possible to calculate the waves transmitted and reflected at each interface. The evaluation of the transmitted and the reflected waves is obtained, both in the backward and forward propagation directions, by imposing the continuity of the EM field components at the interfaces between different dielectric layers. The overall EM field in the structure is given by the superposition of all the reflected and the transmitted waves calculated at each propagation step. The algorithm proceeds until the convergence criterion is met, i.e., the change of the EM field, at the generic ith iteration, in the output section is less than a given tolerance ε (in the analyzed cases $\varepsilon = 10^{-5}$) [19]: $(E_i - E_{i-1})/E_i < \varepsilon$.

In addition, the interaction of the injected current with the active materials is accounted by introducing the rate equations [19]. The material gain $g(x, y, z, \sigma, \lambda)$, which is function of the spatial coordinates x, y, z, of the charge density σ and of the wavelength λ, is obtained from the calculation of the electronic structure of $Ga_{0.77}In_{0.23}N_{0.03}As_{0.97}/Ga_{0.8}In_{0.2}As$ QWs. This was performed in the context of the Band Anticrossing Model to account for the N-induced nonparabolicity of the conduction band, and the 6×6 LK Hamiltonian for the valence bands accounting for the valence band mixing and the strain effects [22]. The electronic bandstructure is used in Fermi's Golden rule (free-carrier theory) to yield material gain [22]. In this way, the bandstructure effects are taken into account rigorously in the EM simulations.

The following expression of the rate equation was used in the stationary analysis [31]:

$$D_e \nabla^2 \sigma(x, y, z) = -\frac{J(z)}{e d_a} + \frac{g(x, y, z, \sigma)}{ehv} \Gamma |E(x, y, z)|^2 + A\sigma + B\sigma^2 + C\sigma^3 \tag{1}$$

where $\sigma(x, y, z)$ is the charge density distribution, d_a is the active layer thickness, $|E(x, y, z)|$ is the electric field modulus; $h = 6.626 \cdot 10^{-34}$ J $\cdot$ s is the Planck constant, $e = 1.602 \cdot 10^{-19}$ C is the electron charge, the product hv is the photon energy expressed in eV, J is the injected current density, and $\Gamma = 0.044$ is the optical confinement factor which was estimated according to the averaging procedure reported in [36] and quantifies how much the optical mode is confined in the active layers. The coefficient Γ was assumed constant since it mainly depends on the number of QWs, whereas the modal profile and, therefore, the optical confinement does not significantly change in the considered wavelength range. Moreover, $A = 2 \cdot 10^8$ s^{-1}, $B = 7 \cdot 10^{-17}$ m^{3}s^{-1}, and $C = 4 \cdot 10^{-41}$ m^{6}s^{-1} are the nonradiative, radiative, and Auger recombination coefficients, respectively, $D_e = 0.001$ m^{2}s^{-1} is the diffusion coefficient, and $g(x, y, z, \sigma)$ is the material gain [22], [32]. For the sake of compact notation, we omit, in (1) and in the following, the dependence on the wavelength of the relevant quantities such as the material gain, the EM field, and the refractive index.

In order to simplify the numerical model and to reduce the computational effort required, the 3-D ridge waveguide structure was reduced to a 2-D one according to the refractive effective index method (REIM) [37]. The REIM was demonstrated to agree well with analytical solutions and with

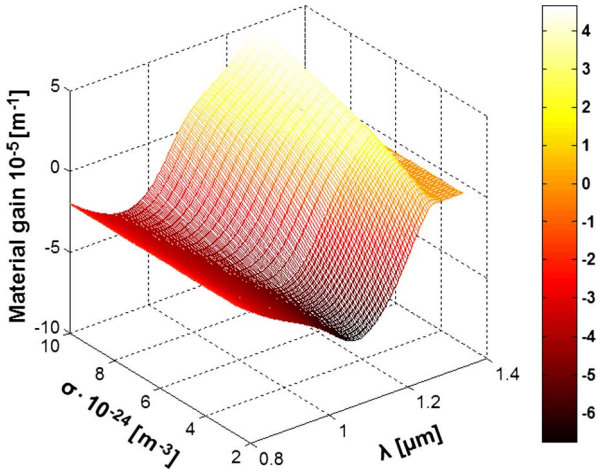

Fig. 1. Material gain as a function of charge density σ and wavelength λ for $Ga_{0.77}In_{0.23}N_{0.03}As_{0.97}/Ga_{0.8}In_{0.2}As$ QW.

other bidimensional and 3-D numerical methods (i.e., finite-element method, mode matching, etc.) [38], [39].

The electric field $E(x, y, z)$ propagating along the waveguiding device was then calculated from the solution of the scalar wave equation

$$\nabla^2 E(x, y, z) + k_0 n^2(x, y, z) E(x, y, z) = 0 \tag{2}$$

where k_0 is the vacuum wavenumber, and $n(x, y, z)$ is the complex refractive index. In the active medium, the complex refractive index $n_a(x, y, z)$ was calculated as [31]

$$n_a(x, y, z) = n_p + \beta_e \, \sigma(x, y, z) + j \frac{g(x, y, z, \sigma)}{2k_0} \tag{3}$$

where n_p is the refractive index of the active medium when the charge injection is absent, and $\beta_e = -1.8 \cdot 10^{-26}$ m^3 is the antiguide coefficient.

In order to allow the step-by-step solution, in a straightforward manner, of the rate equation (1) and of the wave equation (2) within the MoL-BBPM algorithm, the material gain, shown in Fig. 1 as a function of the charge density σ and of the wavelength λ, was approximated through the following expression valid below the material gain saturation:

$$g(x, y, z, \sigma, \lambda) = a_2(\lambda)\sigma^2(x, y, z) + a_1(\lambda)\sigma(x, y, z) + a_0(\lambda). \tag{4}$$

The coefficients a_2, a_1, and a_0, reported in Table 1, are determined at each wavelength to achieve the best fitting of the theoretical material gain as a function of the carrier density. In particular, the coefficients a_0, a_1, and a_2 of the second-order fitting polynomial were calculated, at each wavelength, on the basis of the minimization of the least square error. Considering the behavior of the material gain as a function of the carrier density, the slope of the material gain curve decreases with the charge densities. This behavior was taken into account in the approximation with a constant value that represents the maximum gain saturation value.

As an example, Fig. 2(a) and (b) shows the theoretical material gain (solid curve) and the approximating curve (dashed curve) as a function of the charge density σ and of the wavelength λ, respectively. In particular, Fig. 2(a) pertains to the wavelength fixed value $\lambda = 1.285$ μm, whereas Fig. 2(b) corresponds to the charge density fixed value $\sigma = 3.6 \cdot 10^{24}$ m^{-3}.

TABLE 1

Coefficients a_0, a_1, and a_2 of the approximation of the theoretical material gain, according to (4), for different wavelength values

Wavelength [μm]	a_0 [m^{-1}]	a_1 [m^2]	a_2 [m^5]
1.2507	$-6.0811 \cdot 10^5$	$2.0942 \cdot 10^{-19}$	$-1.1162 \cdot 10^{-44}$
1.2548	$-5.7143 \cdot 10^5$	$2.0185 \cdot 10^{-19}$	$-1.0643 \cdot 10^{-44}$
1.2589	$-5.3579 \cdot 10^5$	$1.9447 \cdot 10^{-19}$	$-1.0130 \cdot 10^{-44}$
1.2631	$-5.0121 \cdot 10^5$	$1.8726 \cdot 10^{-19}$	$-9.6254 \cdot 10^{-45}$
1.2673	$-4.6758 \cdot 10^5$	$1.8015 \cdot 10^{-19}$	$-9.1261 \cdot 10^{-45}$
1.2716	$-4.3460 \cdot 10^5$	$1.7296 \cdot 10^{-19}$	$-8.6261 \cdot 10^{-45}$
1.2759	$-4.0171 \cdot 10^5$	$1.6532 \cdot 10^{-19}$	$-8.1121 \cdot 10^{-45}$
1.2802	$-3.6787 \cdot 10^5$	$1.5664 \cdot 10^{-19}$	$-7.5595 \cdot 10^{-45}$
1.2845	$-3.3139 \cdot 10^5$	$1.4591 \cdot 10^{-19}$	$-6.9275 \cdot 10^{-45}$
1.2888	$-2.8993 \cdot 10^5$	$1.3169 \cdot 10^{-19}$	$-6.1587 \cdot 10^{-45}$
1.2932	$-2.4145 \cdot 10^5$	$1.1265 \cdot 10^{-19}$	$-5.2011 \cdot 10^{-45}$
1.2977	$-1.8707 \cdot 10^5$	$8.9084 \cdot 10^{-20}$	$-4.0738 \cdot 10^{-45}$

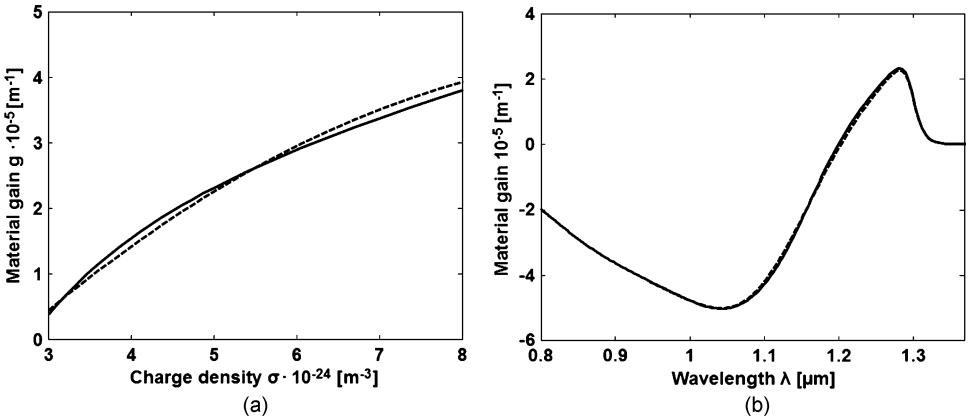

Fig. 2. Theoretical material gain (solid curve) and approximating curve (dashed curve) as a function of the charge density σ at $\lambda = 1.285$ μm (a) and of the wavelength λ at $\sigma = 3.6 \cdot 10^{24}$ m^{-3} (b).

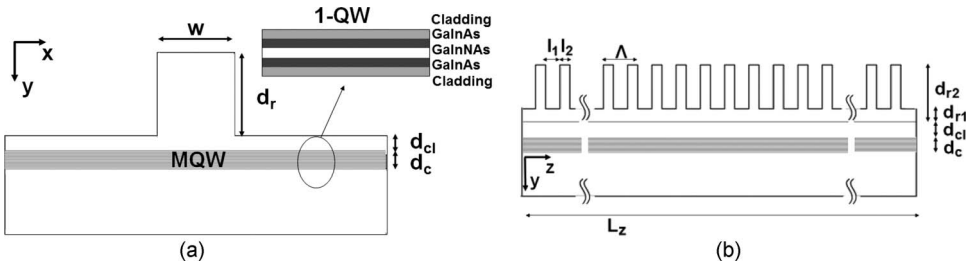

Fig. 3. Scheme of the proposed active switch: (a) transversal section; (b) longitudinal section.

3. Active Photonic Band-Gap Structure

In Fig. 3, the examined device is sketched. Fig. 3(a) shows the transversal section of the active waveguiding structure constituted by a ridge waveguide, the core of which is made of four

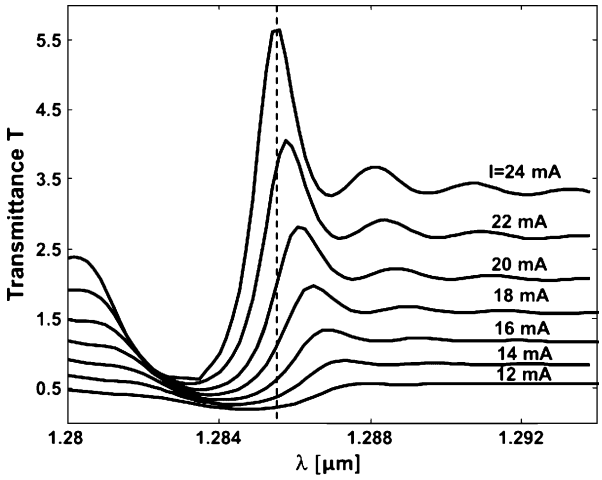

Fig. 4. Spectra of the transmittance T for different values of the injected current $I = 12 - 24$ mA. The dashed vertical line corresponds to the wavelength value $\lambda = 1.2855$ μm for which the transmittance is maximum for $I = 24$ mA.

$Ga_{0.77}In_{0.23}N_{0.03}As_{0.97}$ QWs with refractive index $n_{GaInNAs} = 3.65$ and thickness $d_{GaInNAs} = 7$ nm, with $Ga_{0.8}In_{0.2}As$ barrier layers with refractive index $n_{GaInAs} = 3.47$ and thickness $d_{GaInAs} = 16.5$ nm. The QW was taken into account both in the rate equation (2), by the material gain, and in the EM propagation by the effective refractive index, calculated according to the REIM. Moreover, this particular QW arrangement yields polarization-insensitive performance [22].

The ridge waveguide is characterized by the other following geometrical and physical parameters at the operating wavelength $\lambda_B = 1.2894$ μm [22]: active core with thickness $d_c = 110.5$ nm, cladding layer with refractive index $n_{AlGaAs} = 3.285$ and thickness $d_{cl} = 0.220$ μm, and ridge width $w = 2$ μm. Fig. 3(b) shows the longitudinal section of the simulated structure patterned with a grating having $N = 1003$ alternating ridge waveguide layers. In particular, the grating unit cell has ridge heights of the first and second layers $d_{r1} = 0.1$ μm and $d_{r2} = 1.0$ μm, respectively, and lengths of the first and second layers are $l_1 = 0.120$ μm and $l_2 = 0.076$ μm, respectively.

4. Active Device Operation Under Current Control

In Fig. 4, the spectra of the transmittance T for different values of the injected current are shown. The transmittance T was calculated according to the following definition:

$$T = \frac{I_T}{I_{IN}}$$

where I_T is the intensity of the optical field transmitted at the output port, and I_{IN} is the intensity associated to the input signal. The intensities were calculated as

$$I_i = \int |E_i(x)|^2 dx$$

where E_i is the electric field, and the subscript i refers to the input and the transmitted waves. Owing to the amplification effect of the optical signal, due to the injection of current, the value of the transmittance T can be higher than unity.

Due to the periodic grating, we can notice the occurrence of the PBG, which we define, in the case of a wholly active periodic structure, as the wavelength interval centered at the wavelength of minimum transmittance, i.e., the Bragg wavelength, and delimited by the two adjacent relative maxima (i.e., the band edges). Owing to the refractive index change caused by the charge density

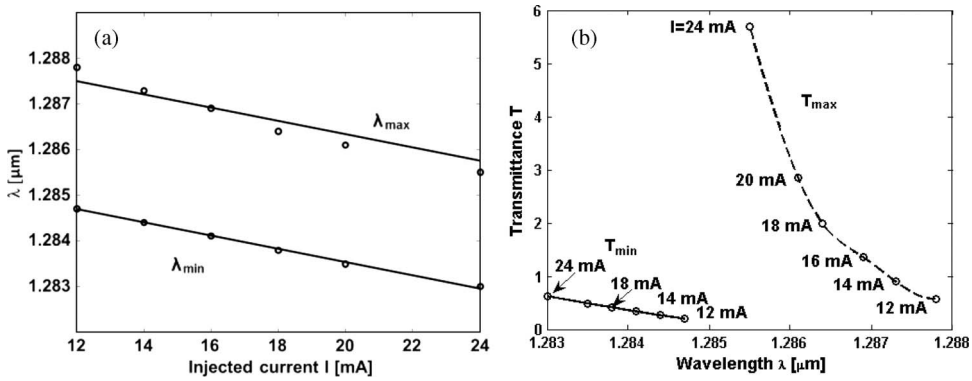

Fig. 5. (a) λ_{max} values of the maximum band edge and Bragg wavelength λ_{min} values in the band gap as a function of the injected current I. (b) Spectra of the maximum T_{max} and the minimum T_{min} transmittance as a function of the corresponding λ values for different injected current I values.

variation, the PBG shifts toward lower wavelength values as the injected current increases from $I = 12$ mA to $I = 24$ mA. This range of variability for the injected current corresponds to current density values comparable with those typically reported for other applications such as SOAs and ridge laser diodes [22], [24].

In particular, Fig. 5(a) shows the behavior of the wavelength λ_{max} of the maximum transmittance T_{max} and of the wavelength λ_{min} of the minimum transmittance T_{min} as a function of the injected current I. Considering the transmittance spectra shown in Fig. 4, the maximum transmittance T_{max} occurs in correspondence of the right band edge of the photonic band gap. Moreover, the Bragg wavelength, i.e., the wavelength λ_{min} where the minimum transmittance occurs, experiences a wavelength shift due to the refractive index change induced by the injected current I.

In Fig. 5(a), we can also see that, by increasing the injected current, both the λ_{min} and λ_{max} values move toward lower wavelength values assuming an almost linear trend with a slope equal to $-0.145 \cdot 10^{-3}$ μm/mA. In addition, Fig. 5(b) reports the patterns of the T_{min} (solid curve) and T_{max} (dashed curve) values as a function of the corresponding λ_{min} and λ_{max} values, whereas the circles indicate some of the injected current values. It is apparent that, by increasing the injected current from 12 mA to 24 mA, the T_{min} values increase from 0.20 to 0.62 (the corresponding λ_{min} values shift from 1.2847 μm to 1.2830 μm), and the T_{max} values increase from 0.57 to 5.69 (the corresponding λ_{min} values shift from 1.2878 μm to 1.2855 μm). Moreover, for $I \geq 14.2$ mA, the maximum transmittance is greater than 1, because the gain due to the injected current is greater than the loss contribution.

From the findings in Figs. 4 and 5, we can infer that the examined PBG waveguiding structure can act as an active switch under current control. In fact, for $\lambda = 1.2855$ μm (dashed vertical line in Fig. 2), the transmittance increases from $T_{OFF} = 0.23$ to $T_{ON} = 5.69$ as the injected current varies from 12 mA to 24 mA, respectively, thus switching from the OFF- to ON-states. This switch exhibits crosstalk $CT = 10\log(T_{OFF}/T_{ON}) = -14.1$ dB, gain in the ON-state $G = 7.6$ dB, contrast ratio $CR = T_{ON}/T_{OFF} = 24.7$, modulation depth $MD = 1 - T_{OFF}/T_{ON} = 0.96$, and the bandwidth for which $CT \leq -10$ dB is $\Delta\lambda_{-10\,dB} = 1.5$ nm. These parameters assure that it is possible at the receiver to distinguish between the two ON- and OFF-states (i.e., to distinguish whether the transmitted bit is zero or one).

Fig. 6 shows the pattern of the transmittance T calculated at the wavelength value $\lambda = 1.2855$ nm as a function of the injected current. We can see that, by fixing the injected current $I = 24$ mA in the ON-state, better switching performance can be obtained for those I values in the OFF-state for which the transmittance is almost equal to zero. It is evident that greater gain G in the ON-state can be obtained for higher I values, whereas for $I \geq 27$ mA, the transmittance reaches its maximum, with a transmittance saturation effect, corresponding to gain value

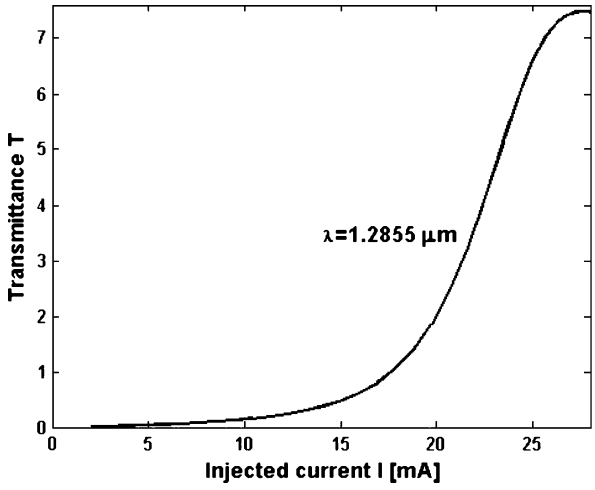

Fig. 6. Transmittance T as a function of the injected current I for $\lambda = 1.2855$ μm.

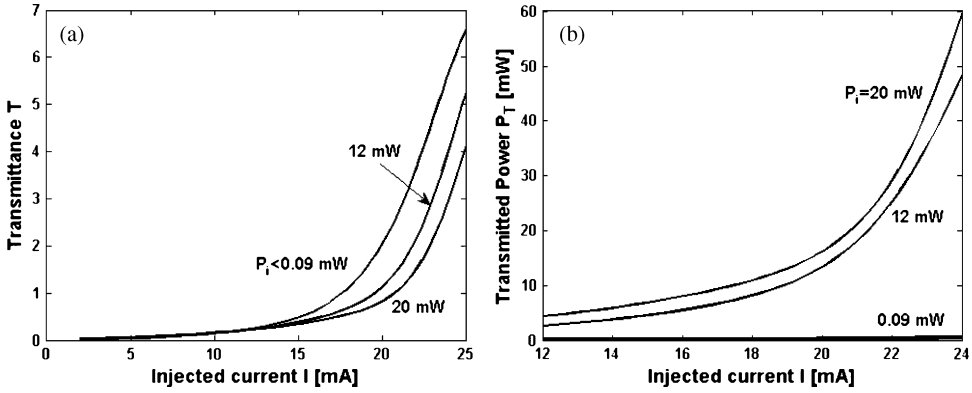

Fig. 7. Curves of the (a) transmittance T and of the (b) transmitted power P_T as a function of the injected current I for the wavelength value $\lambda = 1.2855$ μm and for three different input power values.

$G = 8.8$ dB, due to the different superposition of various contributions such as the material gain value and the shift of the transmittance peak and of the PBG.

5. Influence of the Optical Saturation

A further parameter that influences the switching behavior of the proposed active device is the optical input power P_i. In fact, to parity of injected current, the optical input power and, therefore, the electric field modulus can affect drastically the solution of the rate equation (1). When the P_i value is increased over a certain optical threshold P_{th}, a detriment of the optical gain occurs. This phenomenon, known as gain saturation effect, causes, on one hand, the reduction of the maximum transmittance and, on the other hand, it gives a wavelength shift of the transmittance peak. We have calculated that, for the chosen injected current values, the optical threshold assumes a value equal to about $P_{th} = 0.09$ mW. To evaluate how gain saturation affects the switching mechanism, we report in Fig. 7 the patterns of the transmittance T [see Fig. 7(a)] and of the corresponding transmitted power P_T [see Fig. 7(b)] as a function of the injected current for different values of the input power P_i. It is evident in Fig. 7(a) that, for $P_i > P_{th}$, the T decreases thus adversely affecting the switching performance. This is better demonstrated if we calculate the crosstalk between the

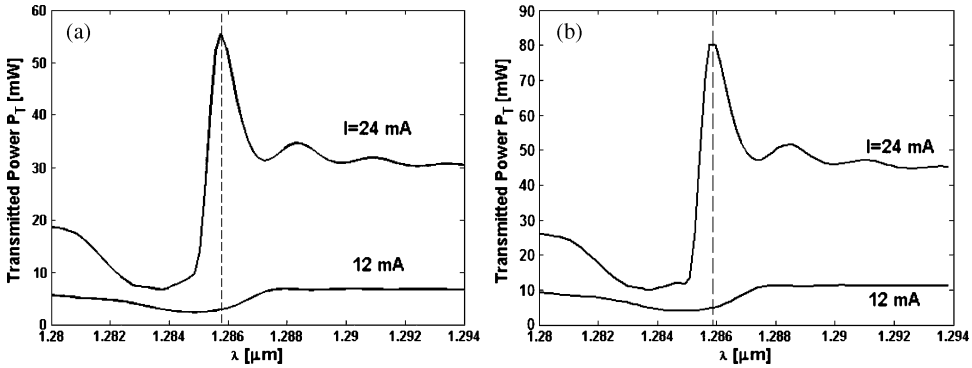

Fig. 8. Spectra of the transmitted power P_T for the values of the injected current $I = 12$ mA and $I = 24$ mA, corresponding to the OFF- and the ON-states, respectively, for the input power (a) $P_i = 12$ mW and (b) $P_i = 20$ mW. The dashed vertical line corresponds to the wavelength values $\lambda = 1.2858$ μm and $\lambda = 1.2859$ μm for which P_T is maximum in the ON-state ($I = 24$ mA) for $P_i = 12$ mW and $P_i = 20$ mW, respectively.

two OFF- ($I = 12$ mA) and ON-states ($I = 24$ mA) for different P_i values. For $P_i = 0.09$ mW, $P_i = 12$ mW, and $P_i = 20$ mW, we have calculated CT $= -14.1$ dB, CT $= -12.8$ dB, and CT $= -11.5$ dB, respectively. Switching performance is not only deteriorated by the suppression of CT for $P_i > P_{th}$ but also by the decrease of gain G $= 7.6$ dB, G $= 6$ dB, and G $= 4.5$ dB for $P_i = 0.09$ mW, $P_i = 12$ mW, and $P_i = 20$ mW, respectively.

Moreover, to parity of injected current by increasing the input power above the threshold value, the spectrum of the transmitted power shifts toward greater wavelength values. This occurrence is evident in Fig. 8, which illustrates the spectra of the transmitted power for input power (a) $P_i = 12$ mW and (b) $P_i = 20$ mW for both the values of the injected current in the OFF- ($I = 12$ mA) and ON-states ($I = 24$ mA). The spectra in Fig. 8 show an enhancement of gain at the photonic band edges, coherently with the experimental demonstration reported in [40] and [41]. This occurrence is due to the reduction of the group velocity v_g of the propagating EM signal and to the consequent enhancement of the interaction between the EM field and the active material [18], [19].

We can see in Fig. 8(a) that, for $P_i = 12$ mW, the maximum of the transmitted power $P_{ON} = 55.4$ mW for $I = 24$ mA occurs at the right band edge of the PBG for $\lambda = 1.2858$ μm, whereas for $I = 12$ mA, the power transmitted at $\lambda = 1.2858$ μm is $P_{OFF} = 2.9$ mW. We can notice that, for $P_i = 12$ mW, the switching mechanism from the OFF- to ON-states and vice versa occurs at $\lambda = 1.2858$ μm with a crosstalk CT $= -12.8$ dB, gain in the ON-state G $= 6.6$ dB, contrast ratio CR $= 18.9$, modulation depth MD $= 0.95$, and bandwidth $\Delta\lambda_{-10\,dB} = 1.0$ nm.

Moreover, Fig. 8(b) shows that, in the case of $P_i = 20$ mW, the maximum of the transmitted power $P_{ON} = 80.1$ mW for $I = 24$ mA occurs at the right band edge of the PBG for $\lambda = 1.2859$ μm, whereas for $I = 12$ mA, the power transmitted at $\lambda = 1.2859$ μm is $P_{OFF} = 5$ mW. Therefore, for $P_i = 20$ mW, the switching mechanism from the OFF- to ON-states and vice versa occurs at $\lambda = 1.2859$ μm with a crosstalk CT $= -12$ dB, gain in the ON-state G $= 6$ dB, contrast ratio CR $= 16$, modulation depth MD $= 0.94$, and bandwidth $\Delta\lambda_{-10\,dB} = 0.8$ nm.

Summarizing, the increase of the input power above the threshold value $P_{th} = 0.09$ mW worsens the switching performance. In fact, by increasing the input power from $P_i = 0.09$ mW to $P_i = 20$ mW, the crosstalk value increases from CT $= -14.1$ dB to CT $= -12$ dB, the gain of the ON-state decreases from G $= 7.6$ dB to G $= 6$ dB, the contrast ratio decreases from CR $= 24.1$ to CR $= 16$, and the modulation depth decreases from MD $= 0.96$ to MD $= 0.94$. On the other hand, the bandwidth $\Delta\lambda_{-10\,dB}$ decreases progressively as a function of P_i, thus making the designed switch more wavelength selective. In particular, by increasing the input power from $P_i = 0.09$ mW to $P_i = 20$ mW, the bandwidth decreases from $\Delta\lambda_{-10\,dB} = 1.5$ nm to $\Delta\lambda_{-10\,dB} = 0.8$ nm.

6. Conclusion

The influence of the injected current on the optical propagation characteristics of dilute nitrides' MQW PBG structure has been investigated. In particular, a wavelength selective active switch at the wavelength $\lambda = 1.2855\ \mu$m has been designed. A good value of the crosstalk $CT = 10Log(P_{OFF}/P_{ON}) = -14.1$ dB with a gain in the ON-state equal to $G = 7.6$ dB is achieved. The presence of a narrow band edge delimiting the PBG in the ON-state allows to obtain a strongly wavelength selective switching at $\lambda = 1.2855\ \mu$m for which a crosstalk $CT \leq -10$ dB is assured in the bandwidth $\Delta\lambda_{-10\,dB} = 1.5$ nm. Compared with InP-based active switch reported in [31], for which a device gain $G \cong 4$ dB was demonstrated at wavelength $\lambda = 1.5494\ \mu$m, the proposed dilute nitride QW active switch achieves higher device gain $G = 7.6$ dB at $\lambda = 1.2855\ \mu$m. Moreover, even the crosstalk improves for our examined device decreasing from $CT \cong -11$ dB for the InP switch to $CT = -14.1$ dB for the GaInNAs device.

The influence of the gain saturation effect, due to the increase of the input power above the threshold value, causes the deterioration of the switching performance by reducing the gain G, the modulation depth MD, and the contrast ratio CR, and by increasing the CT. However, the saturation of the gain improves the wavelength selectivity with the reduction of the bandwidth value to $\Delta\lambda_{-10\,dB} = 0.8$ nm.

Acknowledgment

The research has been conducted in the framework of the European Cooperation in Science and Technology ("COST") Action MP0805.

References

[1] M. J. O'Mahony, C. Politi, D. Klonidis, R. Nejabati, and D. Simeonidou, "Future optical networks," *J. Lightw. Technol.*, vol. 24, no. 12, pp. 4684–4696, Dec. 2006.
[2] R. L. Espinola, M.-C. Tsai, J. T. Yardley, and R. M. Osgood, "Fast and low-power thermooptic switch on thin silicon-on-insulator," *IEEE Photon. Technol. Lett.*, vol. 15, no. 10, pp. 1366–1368, Oct. 2003.
[3] A. Yariv, *Optical Electronics in Modern Communications,* 5th ed. New York: Oxford Univ. Press, 1997, pp. 319–322.
[4] C. H. Lee, P. S. Mark, and A. P. De Fonzo, "Optical control of millimeter-wave propagation in dielectric waveguides," *IEEE J. Quantum Electron.*, vol. 16, no. 3, pp. 277–288, Mar. 1980.
[5] G. Calò, A. D'Orazio, and V. Petruzzelli, "Broadband Mach–Zehnder switch for photonic networks on chip," *IEEE J. Lightw. Technol.*, vol. 30, no. 7, pp. 944–952, Apr. 2012.
[6] K. Stubkjaer, "Semiconductor optical amplifier-based all-optical gates for high-speed optical processing," *IEEE J. Sel. Topics Quantum Electron.*, vol. 6, no. 6, pp. 1428–1435, Nov./Dec. 2000.
[7] D. M. Beggs, T. P. White, L. O'Faolain, and T. F. Krauss, "Ultracompact and low-power optical switch based on silicon photonic crystals," *Opt. Lett.*, vol. 33, no. 2, pp. 147–149, Jan. 2008.
[8] D. M. Beggs, T. P. White, L. Cairns, L. O'Faolain, and T. F. Krauss, "Ultrashort photonic crystal optical switch actuated by a microheater," *IEEE Photon. Technol. Lett.*, vol. 21, no. 1, pp. 24–26, Jan. 2009.
[9] D. M. Beggs, T. Kampfrath, I. Rey, T. F. Krauss, and L. K. Kuipers, "Controlling and switching slow light in photonic crystal waveguides," in *Proc. 13th ICTON*, 2011, pp. 1–4.
[10] J. D. Joannopoulos, R. D. Meade, and J. N. Winn, *Photonic Crystals: Molding the Flow of Light,* 2nd ed. Princeton, NJ: Princeton Univ. Press, 2008.
[11] A. D'Orazio, M. De Sario, V. Marrocco, V. Petruzzelli, and F. Prudenzano, "Photonic crystal drop filter exploiting resonant cavity configuration," *IEEE Trans. Nanotechnol.*, vol. 7, no. 1, pp. 10–13, Jan. 2008.
[12] G. Calò, A. Farinola, and V. Petruzzelli, "Equalization in photonic bandgap multiwavelength filters by the Newton binomial distribution," *J. Opt. Soc. Amer. B*, vol. 28, no. 7, pp. 1668–1679, Jul. 2011.
[13] G. Carlone, A. D'Orazio, M. De Sario, L. Mescia, V. Petruzzelli, and F. Prudenzano, "Design of double-clad erbium-doped holey fiber amplifier," *J. Non-Cryst. Solids*, vol. 351, no. 21–23, pp. 1840–1845, Jul. 2005.
[14] F. Prudenzano, L. Mescia, A. D'Orazio, M. De Sario, V. Petruzzelli, A. Chiasera, and M. Ferrari, "Optimization and characterization of rare-earth-doped photonic-crystal-fiber amplifier using genetic algorithm," *J. Lightw. Technol.*, vol. 25, no. 8, pp. 2135–2142, Aug. 2007.
[15] G. Calò, A. D'Orazio, M. De Sario, L. Mescia, V. Petruzzelli, and F. Prudenzano, "Tunability of photonic band gap notch filters," *IEEE Trans. Nanotechnol.*, vol. 7, no. 3, pp. 273–284, May 2008.
[16] A. D'Orazio, M. De Sario, V. Ingravallo, V. Petruzzelli, and F. Prudenzano, "Infiltrated liquid crystal photonic bandgap devices for switching and tunable filtering," *Fiber Integr. Opt.*, vol. 22, no. 3, pp. 161–172, 2003.
[17] A. R. Cowan and J. F. Young, "Mode matching for second-harmonic generation in photonic crystal waveguides," *Phys. Rev. B*, vol. 65, no. 8, p. 085106, Feb. 2002.

[18] J. M. Bendickson, J. P. Dowling, and M. Scalora, "Analytic expressions for the electromagnetic mode density in finite, one- dimensional, photonic band-gap structures," *Phys. Rev. E, Stat. Phys. Plasmas Fluids Relat. Interdiscip. Topics*, vol. 53, no. 4, pp. 4107–4121, Apr. 1996.
[19] G. Calò, V. Petruzzelli, L. Mescia, and F. Prudenzano, "Study of gain in photonic band gap active InP waveguides," *J. Opt. Soc. Amer. B*, vol. 26, no. 12, pp. 2414–2422, Dec. 2009.
[20] N. Balkan, "The physics and technology of dilute nitrides," *J. Phys., Condens. Matter*, vol. 16, no. 31, Aug. 2004, doi:10.1088/0953-8984/16/31/E01.
[21] B. Royall and N. Balkan, "Dilute nitride n-i-p-i solar cells," *Microelectron. J.*, vol. 40, no. 3, pp. 396–398, Mar. 2009.
[22] D. Alexandropoulos, M. J. Adams, Z. Hatzopoulos, and D. Syvridis, "Proposed scheme for polarization insensitive GaInNAs-based semiconductor optical amplifiers," *IEEE J. Quantum Electron.*, vol. 41, no. 6, pp. 817–822, Jun. 2005.
[23] K. Schires, R. Al Seyab, A. Hurtado, V.-M. Korpijärvi, M. Guina, I. D. Henning, and M. J. Adams, "Optically-pumped dilute nitride spin-VCSEL," *Opt. Exp.*, vol. 20, no. 4, pp. 3550–3555, Feb. 2012.
[24] B. Bonnefont, M. Messant, O. Boutillier, F. Gauthier-Lafaye, A. Lozes-Dupuy, M. V. Sallet, K. Merghem, L. Ferlazzo, J. C. Harmand, A. Ramdane, J. G. Provost, B. Dagens, J. Landreau, O. Le Gouezigou, and X. Marie, "Optimization and characterization of InGaAsN/GaAs quantum-well ridge laser diodes for high frequency operation," *Opt. Quantum Electron.*, vol. 38, no. 4–6, pp. 313–324, Mar. 2006.
[25] V.-M. Korpijärvi, T. Leinonen, J. Puustinen, A. Härkönen, and M. D. Guina, "11 W single gain-chip dilute nitride disk laser emitting around 1180 nm," *Opt. Exp.*, vol. 18, no. 25, pp. 25633–25641, Dec. 2010.
[26] J. Rautiainen, V.-M. Korpijärvi, J. Puustinen, M. Guina, and O. G. Okhotnikov, "Passively mode-locked GaInNAs disk laser operating at 1220 nm," *Opt. Exp.*, vol. 16, no. 20, pp. 15964–15969, Sep. 2008.
[27] M. Kondow, T. Kitatani, K. Nakahara, and T. Tanaka, "Temperature dependence of lasing wavelength in a GaInNAs laser diode," *IEEE Photon. Technol. Lett.*, vol. 12, no. 7, pp. 777–779, Jul. 2000.
[28] J. Hashimoto, K. Koyama, T. Katsuyama, Y. Iguchi, T. Yamada, S. Takagishi, M. M. Ito, and A. Ishida, "1.3 μm travelling-wave GaInNAs semiconductor optical amplifier," *Jpn. J. Appl. Phys.*, vol. 43, no. 6A, pt. 1, pp. 3419–3423, 2004.
[29] M. Kondow, S. Nakatsuka, T. Kitatani, Y. Yazawa, and M. Oka, "Room-temperature pulsed operation of GaInNAs laser diodes with excellent high-temperature performance," *Jpn. J. Appl. Phys.*, vol. 35, no. 11, pp. 5711–5713, 1996.
[30] M. Kondow, T. Kitatani, S. Nakatsuka, M. Larson, K. Nakahara, Y. Yazawa, M. Okai, and K. Uomi, "GaInNAs: A novel material for long-wavelength semiconductor lasers," *IEEE J. Sel. Topics Quantum Electron.*, vol. 3, no. 3, pp. 719–730, Jun. 1997.
[31] G. Calò, A. D'Orazio, M. Grande, V. Marrocco, and V. Petruzzelli, "Active InGaAsP/InP photonic bandgap waveguides for wavelength-selective switching," *IEEE J. Quantum Electron.*, vol. 47, no. 2, pp. 172–181, Feb. 2011.
[32] G. Calò, D. Alexandropoulos, A. D'Orazio, and V. Petruzzelli, "Wavelength selective switching in dilute nitrides multi quantum well photonic band gap waveguides," *Phys. Stat. Sol. (B)*, vol. 248, no. 5, pp. 1212–1215, May 2011.
[33] R. Pregla, "MOL-BPM method of lines based beam propagation method," *Prog. Electromagn. Res.*, vol. 11, pp. 51–102, 1995.
[34] J. Gerdes, "Bidirectional eigenmode propagation analysis of optical waveguides based on method of lines," *Electron. Lett.*, vol. 30, no. 7, pp. 550–551, 1994.
[35] A. D'Orazio, M. De Sario, V. Petruzzelli, and F. Prudenzano, "Bidirectional beam propagation method based on the method of lines for the analysis of photonic band gap structures," *Opt. Quantum Electron.*, vol. 35, no. 6, pp. 629–640, Apr. 2003.
[36] W. Streifer, D. R. Scifres, and R. D. Burnham, "Optical analysis of multiple quantum well lasers," *Appl. Opt.*, vol. 18, no. 21, pp. 3547–3548, Nov. 1979.
[37] T. Makino, "Effective index matrix analysis of distributed feedback semiconductor lasers," *IEEE J. Quantum Electron.*, vol. QE-28, no. 2, pp. 434–440, Feb. 1982.
[38] Working Group I, COST 216, "Comparison of different modeling techniques for longitudinally invariant integrated optical waveguides," *Proc. IEEE*, vol. 136, no. 5, pp. 273–280, Oct. 1989.
[39] D. V. Batrak and S. A. Plisyuk, "Applicability of the effective index method for simulating ridge optical waveguides," *Quantum Electron.*, vol. 36, no. 4, pp. 349–352, 2006.
[40] K. Kuroda, T. Sawada, T. Kuroda, K. Watanabe, and K. Sakoda, "Enhanced spontaneous emission observed at one-dimensional photonic band edges," *J. Opt. Soc. Amer. B*, vol. 27, no. 1, pp. 45–50, Jan. 2010.
[41] K. Inoue, H. Sasaki, and K. Ishida, "InAs quantum-dot laser utilizing GaAs photonic crystal line-defect waveguide," *Opt. Exp.*, vol. 12, no. 22, pp. 5502–5509, Nov. 2004.